Instability of a Mixed Layer Model and the Generation of Near-Inertial Motion. Part I: Constant Mixed Layer Depth

JOHN KROLL

Department of Mathematical Sciences, Old Dominion University, Norfolk, Virginia

(Manuscript received 18 November 1986, in final form 11 December 1987)

ABSTRACT

The stability of Niiler's model of a deepening mixed layer was investigated assuming the deepening rate was negligible. Two basically different instability mechanisms appeared. One is a mixture of a Kelvin–Helmholtz type and parallel flow viscous type with a relatively small horizontal wavelength [O(1 km)]. The other depends on the perturbation of the bulk stress and is related to the inflection point type of instability of an inviscid shear model with a relatively long horizontal wavelength [O(10 km)]. The former instability has its most unstable wave directed generally in the direction of the mean flow, while for the latter, it generally is perpendicular to the mean flow and opposite the wind. Each is likely to produce near-inertial motion. Though the former is potentially stronger than the latter, it is also less likely to occur for usual oceanic conditions.

1. Introduction

There are at least three ways in which the surface can be a local source of downward propagating, near-inertial motion. One way, described by this author (Kroll 1975), is through the Ekman pumping produced by the curl of the wind stress at the surface. This seems to be significant only for unusually strong wind curls.

A second way is shown by Stern (1977) and this author (Kroll 1982) using differing models, to be a large-scale (horizontal scale much larger than mixed layer depth and the scale of turbulence) instability of the mixed layer. This could produce downward propagating near-inertial motion independent of the scale of the wind. This instability is closely related to the overreflection of near-inertial waves from the mixed layer (Stern 1977; Kamachi and Grimshaw 1984). A third way is the interaction of near-inertial waves with a geostrophic shear flow near the surface, either as an instability or overreflection (Tai 1981; Weller 1985; Kunze 1985). The fact that the scale of inertial motion beneath the mixed layer often seems to have no relation to the wind scale (Sanford 1975; Pollard 1980; Pinkel 1983; D'Asaro and Perkins 1984) suggests that the latter two ways should be important.

In this paper we will consider again the second way. The previous model of this author and the model used by both Stern (1977) and Kamachi and Grimshaw (1984) radically differ. They considered an inviscid vertical shear flow at the surface, continuous in velocity and density. My model was two layer and viscous with discontinuities in velocity and density at the mixed layer depth. The most marked difference was the result that my model predicted the most unstable wave in the direction of the mean flow in the mixed layer while theirs was at right angles.

In fact neither model adequately describes a real mixed layer. Hence, we will consider the stability of an actual mixed layer deepening model. We choose that of Niiler (1975), including the extension made by deSzoeke (1980).

We derive the general system of equations that pertain to the problem but consider only the special case for negligible deepening of the mixed layer in this paper. We will deal with the deepening in a subsequent paper. Also in a later paper we will deal with the reflection problem. The previous two papers by this author, Kroll (1982, 1984) are cited extensively, so they will be denoted by (I) and (II) respectively.

2. The model

As in deSzoeke, we consider a mixed layer, as illustrated in Fig. 1, with a transition layer of thickness $2\delta \ll h$ separating the turbulent upper layer from the inviscid interior. We are interested in horizontal scales (L) much greater than the mixed layer depth (h) and the scale of turbulent motions in the mixed layer. We assume that our relatively large-scale perturbations will not interact with the turbulence so that results from our model will be of a different character, the result of a different mechanism, other than the radiation described by Bell (1978).

The equations in the mixed layer, following deSzoeke, for mean (i.e., ensemble averaged over tur-

Corresponding author address: Prof. John E. Kroll, Dept. of Mathematical Sciences, Old Dominion University, Norfolk, VA 23508-8527.

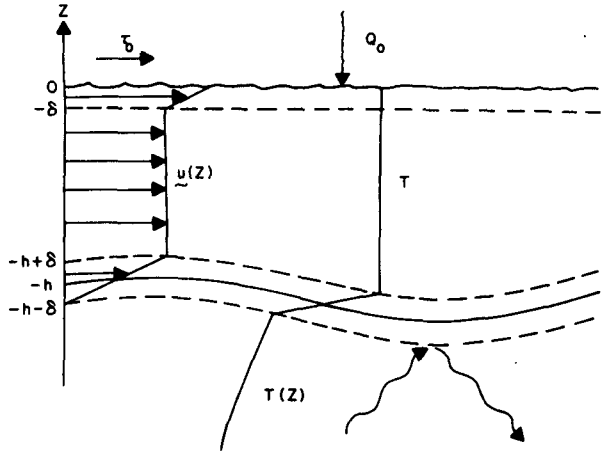

FIG. 1. The model mixed layer.

bulent states) momentum, temperature, turbulent kinetic energy and mass are

$$\mathbf{u}_t + \mathbf{u}\cdot\nabla\mathbf{u} + w\mathbf{u}_z + f\mathbf{k}\times\mathbf{u} = -\frac{1}{\rho_0}\times\nabla p + \frac{1}{\rho_0}\boldsymbol{\tau}_z + \mathbf{H}_m, \quad (1a)$$

$$\rho_0\alpha g T = p_z, \quad (1b)$$

$$T_t + \mathbf{u}\cdot\nabla T + wT_z = Q_z + H_h, \quad (1c)$$

$$e_t + \mathbf{u}\cdot\nabla e + we_z = F_z + \frac{1}{\rho_0}\boldsymbol{\tau}\cdot\mathbf{u}_z - \alpha g Q - \epsilon + H_e, \quad (1d)$$

$$\nabla\cdot\mathbf{u} + w_z = 0, \quad (1e)$$

where ∇ is the horizontal gradient operator; $\mathbf{u}$ the horizontal velocity; w the vertical velocity; p pressure; T temperature; ρ_0 is the reference density. The turbulent vertical fluxes of momentum, heat, and energy are

$$\boldsymbol{\tau} = -\rho_0\overline{u'w'}, \quad Q = -\overline{w'T'} \quad \text{and}$$

$$F = -\overline{w'\left(\frac{p'}{\rho_0} + \frac{1}{2}\mathbf{u}'\cdot\mathbf{u}'\right)};$$

$$e = \frac{1}{2}\overline{\mathbf{u}'\cdot\mathbf{u}'},$$

where ϵ is viscous dissipation, and α is the coefficient of thermal expansion, where turbulent quantities are primed and the overbar indicates an ensemble average. $\mathbf{H}_m$, H_h and H_e are the horizontal gradients of correlations of turbulent quantities. We are assuming hydrostatic balance since we assume $h/L \ll 1$.

Niiler makes empirical assumptions for $\boldsymbol{\tau}$, Q and F to close the system. He assumes $\boldsymbol{\tau}$ and Q are linearly distributed within the mixed layer. This we do, but also add eddy viscosity terms to deal with z-dependence for the perturbations. Hence we assume

$$\boldsymbol{\tau} = \boldsymbol{\tau}_0 + \frac{z}{h}(\boldsymbol{\tau}_0 - \boldsymbol{\tau}_+) + \rho_0 K_v \mathbf{u}_z \quad (2a)$$

$$Q = Q_0 + \frac{z}{h}(Q_0 - Q_+) + K_v' T_z \quad (2b)$$

where subscripts 0 and + mean evaluation at the surface and at the top of the transition layer, respectively. In addition, we assume that $\mathbf{H}_m$ and H_h are given by semi-empirical expressions $K_H\nabla^2\mathbf{u}$ and $K_H'\nabla^2 T$, respectively. In some instances we add a mean-square drag term $-C_D|\mathbf{u}|\mathbf{u}$ to $\mathbf{H}_m$. We include horizontal eddy viscosity to deal with short wavelengths and mean-square drag to deal with long wavelengths. H_e can also be expressed in a similar manner, but eventually will be neglected.

We integrate (1e) across the transition layer (remembering $h = h(x, y, t)$), let $\delta \to 0$ and find that $\nabla h\cdot\mathbf{u} + w$ is conserved across the layer. This means

$$(h_t + \mathbf{u}\cdot\nabla h + w)_+ = (h_t + \mathbf{u}\cdot\nabla h + w)_- \equiv H \quad (3a)$$

where subscript $(-)$ represents the value at the bottom of the transition layer. Integrating (1a) and (1c) similarly yields for $H \geq 0$

$$\frac{\Delta\boldsymbol{\tau}}{\rho_0} = H\Delta\mathbf{u} \quad \text{and} \quad (3b)$$

$$\Delta Q = H\Delta T \quad (3c)$$

where $\Delta(\ ) = (\ )_+ - (\ )_-$ is a jump of quantity $(\ )$ across the transition layer. For $H < 0$, we assume no unmixing or detraining implying $\Delta\boldsymbol{\tau} = \Delta Q = 0$. Layer dissipation terms would also appear but have been neglected since they will eventually involve only products of perturbed quantities.

We should note that in deriving (3a, b, c) we let the limit of

$$\int_{-h-\delta}^{-h+\delta}\mathbf{u}\,dz$$

and other similar integrals vanish as $\delta \to 0$ since we have a viscous fluid. For the inviscid shear model of Stern these limits do not vanish for a slab flow (a step function for the steady state mixed layer flow). Thus, how we treat these limits is important. In our model the effect of the $w\mathbf{u}_z$ term of the momentum equation in the transition layer, important for an inflection point instability in the inviscid shear model, is suppressed. Thus we might expect no inflection point instability, but we will see we actually do obtain a related instability similar to it.

We integrate (1d) across the transition layer and then from the top of transition layer to surface and add the results to obtain:

$$\int_{-h+\delta}^{0}(e_t+\mathbf{u}\cdot\nabla e)dz+H\Delta e=F_0-F_--\int_{-h-\delta}^{-h+\delta}\epsilon dz-\int_{-h+\delta}^{0}\epsilon dz-\alpha g\left[\int_{-h-\delta}^{-h+\delta}Qdz+\int_{-h+\delta}^{0}Qdz\right]+\frac{1}{\rho_0}\times\left[\int_{-h-\delta}^{-h+\delta}\boldsymbol{\tau}\cdot\mathbf{u}_z dz+\int_{-h+\delta}^{0}\boldsymbol{\tau}\cdot\mathbf{u}_z dz\right]+\int_{-h-\delta}^{0}H_e dz. \tag{4}$$

We now nondimensionalize, letting $(x, y) = L(x', y')$, $z = h_* z'$, $t = f_0^{-1}t'$, $h = h_* h'$, $T = \Gamma h_* T'$, $p = \rho_0 f_0 U_0 L p'$, $(u, v) = U_0(u', v')$, $w = (h_*/L)U_0 w'$, $\boldsymbol{\tau} = \tau^0\boldsymbol{\tau}$, and $Q = Q^0 Q'$, where

$$\Gamma=\frac{N_-^2}{\alpha g}=\frac{d\bar{T}_-}{dz},\quad u_*=\left(\frac{\tau^0}{\rho_0}\right)^{1/2},$$

$$h_*=\frac{u_*}{\sqrt{N_- f_0}},\quad U_0=\tau^0/f_0 h_*\rho_0.$$

Here τ^0 is the magnitude of the surface stress and Q^0 is the maximum magnitude of the heat flux. We assume that before mixed layer deepening the temperature near the surface is linear in z so that buoyancy frequency, N_-, just beneath the mixed layer, remains constant. Pressure is nondimensionalized in a different manner from deSzoeke to make an O(1) term.

We assume that the perturbation wave does not vary in the y-direction and that $\boldsymbol{\tau}_0$ makes an angle θ counterclockwise with the positive x-axis. Then derivatives in y can be neglected. Using (2) and (3) in (1a, 1b, 1c, 1e) and (4) we get the dimensionless equations describing the mixed layer (dropping primes on dimensionless quantities):

$$\mathbf{u}_t+Ru\mathbf{u}_x+Rw\mathbf{u}_z+\mathbf{k}f\times\mathbf{u}=-p_x\mathbf{i}+\frac{\boldsymbol{\tau}_0}{h}-\frac{1}{h}H\Delta\mathbf{u}+E\mathbf{u}_{zz}+\sigma\mathbf{u}_{xx}-\frac{\bar{\sigma}}{h}|\mathbf{u}|\mathbf{u} \tag{5a}$$

$$p_z=\frac{B_-^2}{R}T \tag{5b}$$

$$T_t+RuT_x+RwT_z=\frac{1}{h}\{bQ_0-H\Delta T\}+\sigma T_{xx}+ET_{zz} \tag{5c}$$

$$\frac{1}{2}[h\Delta T-|\Delta\mathbf{u}|^2]H=\frac{F_0-F_-}{h_* f_0 U_0^2}-\frac{1}{2}bh(Q_0+Q_-)+\int_{-h}^{0}\boldsymbol{\tau}\cdot\mathbf{u}_z dz-\int_{-h}^{0}\frac{\epsilon}{f_0 U_0^2}dz+\Delta\mathbf{u}\cdot\boldsymbol{\tau}_- \tag{5d}$$

$$u_x+w_z=0 \tag{5e}$$

where the Ekman numbers E and σ, the drag coefficient $\bar{\sigma}$, the Rossby number R, the Burger number B_-^2, and the heating coefficient b are given by

$$\sigma=\frac{K_H}{f_0 L^2}=\frac{K'_H}{f_0 L^2},\quad E=\frac{K_v}{f_0 h_*^2}=\frac{K'_v}{f_0 h_*^2},\quad R=\frac{U_0}{f_0 L},$$

$$\bar{\sigma}=\frac{N_-}{f_0}C_D,\quad B_-=\frac{h_* N_-}{L f_0},\quad b=\frac{\alpha g Q^0}{u_*^2 N_-},$$

and $f = 1$. The F and ϵ remain dimensional. The interface term, H, is given by (3a). Actually, with the parameterization used, $B_- = R$, but we maintain them as separate entities to compare more easily with results from (I) and (II).

The left side of (4) has been neglected under the assumption that e/U_0^2 and its derivatives in x and t are negligible. The e term in H_e is negligible for the same reason, while other terms in H_e are negligible because $h/L \ll 1$ or will be products of perturbed quantities. The integrals of ϵ and Q across the thin transition layer in Eq. (4) are assumed negligible compared to those across the mixed layer. The variation of ϵ with depth may not be important for the mean flow, but it may be for the perturbation. So, from Alexander and Kim (1976), we use the empirical relations (z-dimensional)

$$\epsilon(z)=\epsilon_M+n_D\beta u_*^3 e^{\beta z}\quad\text{and}\quad F_0=n_G u_*^3 \tag{6}$$

where

$$\epsilon_M\approx 2\times10^{-4}\ \text{cm}^2\ \text{s}^{-3},\quad \beta\approx 0.05\ \text{m}^{-1},$$

$$n_D\approx 1.25,\quad n_G\approx 2.5.$$

We then show (h-dimensional)

$$D=\int_{-h}^{0}\epsilon dz=n_D u_*^3(1-e^{-\beta h})+\epsilon_M h. \tag{7}$$

3. Perturbation of the model

Consider now a perturbation of the mixed layer system, letting $(\ ) = (\bar{\ }) + (\ )'$. For the unperturbed or mean system we obtain

$$\bar{\mathbf{u}}_t+\mathbf{k}f\times\bar{\mathbf{u}}=\frac{\bar{\boldsymbol{\tau}}_0-\Delta\bar{\mathbf{u}}\bar{h}_t}{\bar{h}}-\frac{\bar{\sigma}}{\bar{h}}|\bar{\mathbf{u}}|\bar{\mathbf{u}} \tag{8a}$$

$$\bar{T}_t=\frac{1}{\bar{h}}\{bQ_0-\Delta\bar{T}\bar{h}_t\} \tag{8b}$$

$$\frac{1}{2}[\bar{h}\Delta\bar{T}-|\Delta\bar{\mathbf{u}}|^2]\bar{h}_t=\frac{1}{h_* f_0 U_0^2}[F_0-F_--\bar{D}]-\frac{1}{2}b\bar{h}Q_0+\Delta\bar{\mathbf{u}}\cdot\bar{\boldsymbol{\tau}}_-. \tag{8c}$$

Solutions to these equations will be independent of z with $\bar{w} = 0$. The interior is assumed motionless and nondiffusive, so $\bar{\boldsymbol{\tau}}_- = \bar{\mathbf{u}}_- = 0$, which implies $\Delta\bar{\boldsymbol{\tau}} = \bar{\boldsymbol{\tau}}_+$ and $\Delta\bar{\mathbf{u}} = \bar{\mathbf{u}}_+ = \bar{\mathbf{u}}$, and $(d\bar{T}/dz) = 1$ near the mixed layer in the interior.

The perturbation equations for the mixed layer are (dropping primes on perturbed variables):

$$\mathbf{u}_t + R\bar{u}\mathbf{u}_x + \mathbf{k}f\times\mathbf{u} = -p_x\mathbf{i} - \frac{h}{\bar{h}^2}[\bar{\boldsymbol{\tau}}_0 - \bar{h}_t\bar{\mathbf{u}}]$$

$$-\frac{\bar{\mathbf{u}}}{\bar{h}}H - \frac{1}{\bar{h}}\bar{h}_t\Delta\mathbf{u} + \sigma\mathbf{u}_{xx} + E\mathbf{u}_{zz} - \frac{\bar{\sigma}}{\bar{h}}$$

$$\times\left[|\bar{\mathbf{u}}|\mathbf{u} + \frac{(\bar{\mathbf{u}}\cdot\mathbf{u})}{|\bar{\mathbf{u}}|}\bar{\mathbf{u}} - \frac{h}{\bar{h}}|\bar{\mathbf{u}}|\bar{\mathbf{u}}\right] \quad (9a)$$

$$p_z = \frac{B_-^2}{R}T \quad (9b)$$

$$T_t + R\bar{u}T_x = \frac{-h}{\bar{h}^2}[bQ_0 - \Delta\bar{T}\bar{h}_t] - \frac{1}{h}$$

$$\times\{\Delta T\bar{h}_t + \Delta\bar{T}H\} + \sigma T_{xx} + ET_{zz} \quad (9c)$$

$$\frac{1}{2}[\bar{h}\Delta\bar{T} - |\bar{\mathbf{u}}|^2]H + \frac{\bar{h}_t}{2}[\bar{h}\Delta T + \Delta\bar{T}h - 2\bar{\mathbf{u}}\cdot\Delta\mathbf{u}]$$

$$= \frac{-h\epsilon(-\bar{h})}{f_0U_0^2} - \frac{1}{2}bQ_0h - \int_{-\bar{h}}^{0}\bar{\boldsymbol{\tau}}\cdot\mathbf{u}_z dz \quad \text{and} \quad (9d)$$

$$u_x + w_z = 0 \quad (9e)$$

where $H = h_t + R(\bar{u}h_x + w)_+$ from (3a) and where $\epsilon(-\bar{h})$ is from (6). We assumed perturbations of the net flux $F_0 - F_-$ are negligible.

The perturbation equations for the interior are the same as in (I) and (II), but with the different scaling:

$$\mathbf{u}_t + \mathbf{k}f\times\mathbf{u} = -\left(p_x - \frac{B_-^2}{R}\Delta\bar{T}h_x\right)\mathbf{i}, \quad (10a)$$

$$p_z = \frac{B_-^2}{R}T, \quad (10b)$$

$$T_t + \left(\frac{B(z)}{B_-}\right)^2 Rw = 0 \quad (10c)$$

$$u_x + w_z = 0. \quad (10d)$$

where $B(z) = (h_*/L)(N(z)/f_0)$ and the buoyancy frequency, $N(z)$, can be allowed to decrease realistically with z as in (I). However, in this paper we will assume $N(z) = N_-$, a constant.

The boundary conditions which must be satisfied for the perturbation system are at $z = 0$: $\mathbf{u}_z = T_z = w = 0$ and at $z = -\bar{h}(t)$: p and $\bar{u}h_x + w$ continuous, (and $\mathbf{u}_z = T_z = 0$ for the mixed layer only). For a stability analysis we need, in addition, the radiation condition that there is not energy coming from $z \to -\infty$.

These unperturbed and perturbed systems of equations and their boundary conditions constitute the system we want to solve. According to Niiler (1975), after about the first half-pendulum day, $\bar{h}$ is approximately 2 and the deepening is relatively slow thereafter, i.e., $\bar{h}_t \ll 1$. This suggests that we may consider $\bar{h}$ constant relative to the time scale of oscillations for $\bar{h} \geq 2$. If $\bar{h}_t$, b and $\epsilon(-h)$ are assumed negligible, one solution in the mixed layer has $T = H = 0$ and $\mathbf{u}$ independent of z. Hence, the conditions at $z = -\bar{h}$ are the kinematic conditions for an interface between two fluids of differing density, $[h_t + R(uh_x + w)]_+ = [h_t + Rw]_- = 0$. Thus, the system evolves into the two-layer system which is almost exactly the same as the one we previously considered (I and II) except for the perturbation of the bulk stress term, $(h/\bar{h}^2)\bar{\boldsymbol{\tau}}_0$, and the mean square drag in (9a).

4. Mean flow solution

The complete mean system will not be solved exactly, though certain parts will. Neglecting the drag term, we can write Eqs. (8a) and (8b) as

$$(\bar{h}\bar{\mathbf{u}})_t + \mathbf{k}f\times\bar{h}\bar{\mathbf{u}} = \boldsymbol{\tau}_0(t) \quad (11)$$

$$\left(\bar{h}\bar{T} + \frac{1}{2}\bar{h}^2\right)_t = bQ_0(t) \quad (12)$$

where $\boldsymbol{\tau}_0$ and Q_0 are applied wind stress and heating at the surface. The effect of the drag will be to attenuate gradually the inertial oscillations. This attenuation should not be important. We consider the flow of the mixed layer only after it has reached a depth h_* and so do not concern ourselves with satisfying any particular initial conditions. We then write a solution of (11) in the form:

$$\bar{h}\bar{\mathbf{u}} = \left(\frac{\tau_0}{f}\sin\theta + a\cos ft, \frac{-\tau_0}{f}\cos\theta - a\sin ft\right), \quad (13)$$

assuming τ_0 varies slowly in time if at all. The magnitudes of τ_0/f and a are usually comparable in the ocean, but can possibly vary greatly relative to each other.

Integrating (12) yields

$$\bar{h}\bar{T} = -\frac{1}{2}[\bar{h}^2 - \bar{h}^2(0)] + \bar{h}(0)\bar{T}(0) + b\int_0^t Q_0 dt, \quad (14)$$

where $\bar{h}(0)$ and $\bar{T}(0)$ are initial depth and temperature. Since $\bar{T}_z = 1$ before mixing, we find $\bar{T}_- = -\bar{h}$, assuming $\bar{T} = 0$ at $z = 0$, and obtain

$$\Delta\bar{T} = \bar{T} - \bar{T}_- = \frac{1}{2}\left[\bar{h} + \frac{\bar{h}^2(0)}{\bar{h}}\right] + \frac{b}{\bar{h}}\int_0^t Q_0 dt + \frac{\bar{h}(0)\bar{T}(0)}{\bar{h}}. \quad (15)$$

Assuming $Q_0 = 0$ and $\bar{h}(0) = 0$, we have simply $\Delta\bar{T} = \frac{1}{2}\bar{h}$.

As previously mentioned, in calculations by Niiler (1975) for the mean system typically the mixed layer deepens quickly over one inertial period to $\bar{h} \approx 2$ and then slows thereafter. So we will assume $\bar{h}_t$ negligible and $\bar{h} \geq 2$. This choice of $\bar{h}$ with our nondimensionalization forces a state of realism absent from (I) and (II).

5. Pertubation solution

The major dimensionless variables and parameters are summarized in Table 1. If any of $\bar{h}_t$, Q_0 or $\epsilon(-\bar{h})$ are nonzero, the system is quite complicated with a numerical solution required in general. If these parameters are zero, then we can have a trivial solution for T and H in (9c) and (9d). We will call this an external solution, since it depends strongly on the interior which is external to the mixed layer. We can also have a nontrivial solution which we will call an internal solution, since it depends only on the internal structure of the perturbation within the mixed layer, independent of the interior.

The internal solution is a modification of a similar set of solutions found in (I) which are always stable. The modification here actually has physical meaning only for $\bar{h}_t > 0$, since $\bar{h}_t = 0$ infers that the perturbation unmixes and detrains the mixed layer, violating (3). So we will consider this internal solution when we subsequently treat the $\bar{h}_t > 0$ case. Hence, in this paper we will consider only the case for $\bar{h}_t = Q_0 = \epsilon(-\bar{h}) = 0$ and $H = T = 0$ from (9c) and (9d).

a. *Exclusion of a steady state oscillation*

Let us consider first the case with no steady state oscillations ($a = 0$). Following the usual stability analysis, as in (I), we assume a solution of the form $(\hat{\ })e^{ikx-i\omega t}$ in the mixed layer and $(\hat{\ })e^{ikx-i\omega t+i\mu z}$ in the interior, where k, μ are dimensionless horizontal and vertical wavenumbers respectively and ω the dimensionless frequency. Solving (9a), (9b) and (9e) for the mixed layer, the equations (10) for the interior and using the boundary conditions at $z = 0$ and the continuity conditions at $z = -\bar{h}$, we obtain

$$\mu\left\{(f_1 f_2 - q_1 q_2)(kR\bar{u} - \omega) + \bar{h}k^2 B_-{}^2 q_2 \Delta\bar{T} - \frac{kR\tau_0}{\bar{h}} \times (iq_2\cos\theta + f_1\sin\theta) + \frac{\bar{\sigma}\tau_0 Rk}{f\bar{h}^2}(iq_2\sin\theta - f_1\cos\theta)\right\} - i\bar{h}k^2 B_-{}^2 q_2 = 0, \quad (16a)$$

where

$$q_1 = q - \frac{i\bar{\sigma}\tau_0}{f\bar{h}^2}(1 + \sin^2\theta),$$

$$q_2 = q - \frac{i\bar{\sigma}\tau_0}{f\bar{h}^2}(1 + \cos^2\theta),$$

$$f_{1,2} = f \pm \frac{1}{2}\frac{\bar{\sigma}\tau_0}{f\bar{h}^2}\sin 2\theta, \quad q = kR\bar{u} - \omega - i\sigma k^2,$$

$$\mu^2 = B_-{}^2 k^2/(\omega^2 - f^2)$$

and $\bar{u} = \tau_0 \sin\theta/f\bar{h}$ from (13) for $a = 0$. The proper root for μ is determined by the radiation condition that there be no energy coming from $z \to -\infty$, i.e., $\mathrm{Re}(\omega\mu) \geq 0$ as in (I). If we set $\bar{\sigma} = 0$, then this simplifies to

$$\mu\left\{(f^2 - q^2)(kR\bar{u} - \omega) + \bar{h}k^2 B_-{}^2 q\Delta\bar{T} - \frac{kR\tau_0}{\bar{h}}(iq\cos\theta + f\sin\theta)\right\} - i\bar{h}k^2 B_-{}^2 q = 0. \quad (16b)$$

Equation (16b) is equivalent to the result in (I) [Eq. (7)] except for the perturbation of the stress term (last term inside the brackets). We consider (16a) an equation for the eigenfrequency $\omega = \omega_r + i\omega_i$ as a function of the independent variables k and θ and parameters $B_-, R, \bar{h}, \Delta\bar{T}, \sigma$ and $\bar{\sigma}$. For our nondimensionalization, $\tau_0 = 1$, $B_- = R$, and $\Delta\bar{T}$ is actually a function of $\bar{h}$ from (15), but it is convenient in our analysis to relax these restrictions in some instances which will be explicitly stated. The objective is to determine under what conditions we have instability, i.e., $\omega_i > 0$.

We do not know the best value for K_H. Brown and Owens (1982), investigating the interaction of internal waves and mesoscale eddy motion found $K_H \sim 10^6$ cm^2 s^{-1}. This was not in the mixed layer where it very well could be larger. But on the other hand, the shorter wavelengths of interest here [O(1 km)] are considerably less than mesoscale, so an estimate of 10^6 cm^2 s^{-1} would seem as good as any. The assumption of $C_D \sim O(10^{-3})$ is used almost universally. Realistic nominal values of our parameters are $R = 2.0$, $\sigma = 1.0$ and $\bar{\sigma} = 0.1$, based on $L = 1$ km, $\tau_0/\rho_0 = 2$ cm^2 s^{-2}, $N_-/f_0 = 200$, $K_H = 10^6$ cm^2 s^{-1} and $C_D = 0.5 \times 10^{-3}$

TABLE 1. Summary of major dimensionless parameters.

$\Delta\bar{T}$	temperature jump across transition layer for the mean state
B	$\frac{h_*}{L}\frac{N(z)}{f_0}$, where $h_* = \frac{u_*}{\sqrt{N_- f_0}}$, $u_* = \left(\frac{\tau^0}{\rho_0}\right)^{1/2}$ and B^2 is a Burger number
B_-	$\frac{h_*}{L}\frac{N_-}{f_0}$, where $N_- = N$ at bottom of transition layer
R	$\frac{U_0}{f_0 L}$ is the Rossby number. $U_0 = \tau^0/f_0 h_* \rho_0$
σ	$\frac{K_H}{f_0 L^2}$ is the horizontal Ekman number assumed the same for heat
E	$\frac{K_v}{f_0 h_*^2}$ is the vertical Ekman number assumed the same for heat
b	$\alpha g Q^0/u_*^2 N_-$, heating coefficient
$\bar{\sigma}$	$N_- C_D/f_0$, a drag coefficient
$\bar{h}_t$	deepening rate
ω	wave frequency (nondimensionalized by f_0) $= \omega_r + i\omega_i$
k	horizontal wavenumber nondimensionalized by L^{-1}
μ	vertical wavenumber $= B_- k/\sqrt{\omega^2 - f^2}$
a	parameter partitioning steady and oscillating components of mean flow from Eq. (13)
θ	angle between direction of the wind and direction of the wave perturbation

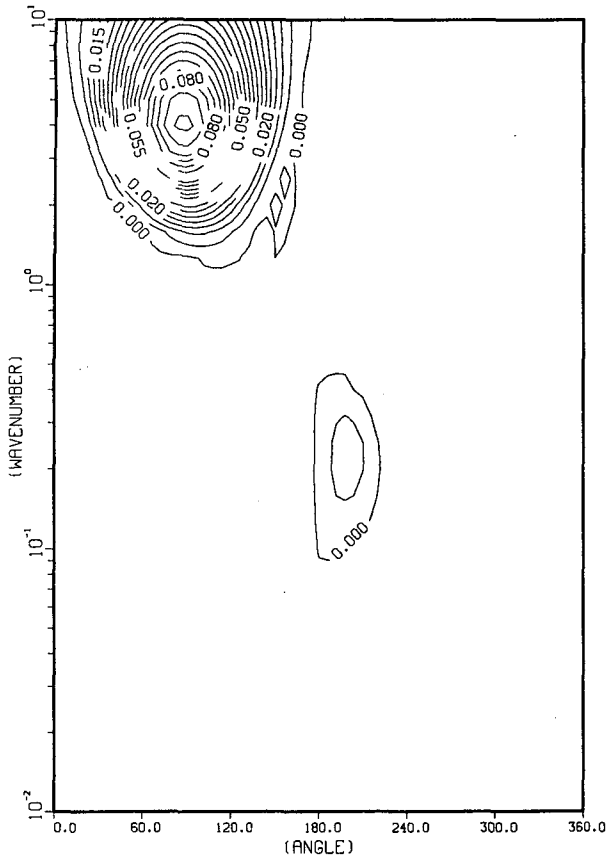

FIG. 2. Contours of positive ω_i in (θ, k) space for $R = \bar{h} = 2.0$, $\Delta\bar{T} = 0.0$, $\sigma = 1.0$ and $\bar{\sigma} = 0.1$. Contours have 0.005 intervals.

which implies $h_* \approx 10$ m for $f_0 \approx 10^{-4}$ s^{-1}. Also $\bar{h} = 2$ and $\Delta\bar{T} = 0.5\bar{h}$.

We are interested in near-inertial motion which is defined to have a frequency within a few percent of f. By this definition some of our results will not be near-inertial. But in a broader sense they are. For example, a wave packet directed poleward from a latitude of 20° with $\omega = 2$, which is not near-inertial, will reach a turning latitude at about 43° where it will be near-inertial and have its amplitude increased (see Kroll 1975). Thus motion, which would not be considered near-inertial at its source, ends up being near-inertial and the generation of such motion is of interest here.

On Fig. 2 are plotted positive (unstable) contours of ω_i in (θ, k) space for $R = \bar{h} = 2.0$, $\Delta\bar{T} = 0.0$, $\sigma = 1.0$, and $\bar{\sigma} = 0.1$ using (16a). The figure clearly shows that there are two centers of instability. The most unstable wave for one is centered around $\theta = 90°$ with $\omega \approx 2.2 + 0.1i$ and $k = 4$ which for our parameter values corresponds to a wavelength, $\lambda = 2\pi L/k$, around 2 km. The other is centered around $\theta = 195°$ with $\omega \approx 1.0 + 0.07i$ and $k = 0.2$ which corresponds to a wavelength around 30 km. We will call these instabilities the short-wave and long-wave instabilities, respectively.

For the stability of the laminar Ekman layer, Lilly (1966) found two types of instability mechanisms, the viscous parallel flow type and the inviscid inflection point type. From (I) we determined that our short-wave instability corresponded to the former type. However, the possibility of the latter type in our model has been suppressed in deriving the two layer model. Yet surprisingly, we still have the instability whose properties we can show are very similar to this latter type which is also the type of Stern (1977) and Kamachi and Grimshaw (1984). Let us look at each of our instabilities.

The short-wave instability corresponds to the parallel flow type and is the same as that investigated in (I) if the stress perturbation is neglected. This neglect does not change the basic features. The parameters α and B_0 in that paper in terms of our present parameters are given by $B_0 = \bar{h}B_-$ and $\alpha = \bar{h}\Delta\bar{T}B_-$, with R there being $R/\bar{h}$ in terms of the present definition of R.

In (I) our investigation showed that this instability is not a continuation of the classical Kelvin–Helmholtz instability, that an increase in vertical radiation increased the instability and, for the limiting case $\Delta\bar{T} = 0$ and $\sigma \to 0$, $k > 2f\bar{h}/R$ for instability. Recently it was discovered that the character of this instability is related to the work of Ostrovskiy and Tsimring (1981). Their two-layer model is inviscid, nonrotating and unbounded top and bottom, but the character of the instability is similar in that an increase in vertical radiation increases the instability which is not the case for classical Kelvin–Helmholtz instability. To explain this, they use the concept of negative energy which states that any mechanism that removes energy from the system can increase the negativeness of a mode having negative energy leading to its instability.

Let us apply this concept to our instability. We use Ostrovskiy and Tsimring, and especially the work of Cairns (1979). On Fig. 3 we show the real part of ω versus k for two of the solutions of (16b) for $\theta = 90°$, $\Delta\bar{T} = \sigma = 0$, $B_- = 2$, $R = \bar{h} = 1$. The curves marked 1 and 2 are neutral modes. The portion of curve 1 for $k < 2$ has a solution that grows with increasing depth. This would be what is called a "leaky wave" by Ostrovskiy and Tsimring. For $\sigma > 0$ it can be shown that this mode is a stable, downward propagating wave.

The energy of a given mode is defined as the difference between the energy of the system with the mode present and that of the mean system without the mode, averaged over one horizontal wavelength. With respect to the motionless interior the energy of mode (1) is positive and of mode (2) positive for $\omega < 0$ and negative for $\omega > 0$. The negative portion of mode (2) coalesces with the positive mode (1) after $k = 3$ to form an unstable mode. Benjamin has classified this type a class C instability, which is a Kelvin–Helmholtz type. (But for our case it is not the classical Kelvin–Helmholtz instability.)

There is another type of instability here. As σ is increased from 0, the portion of mode (1) for $k > 2$ be-

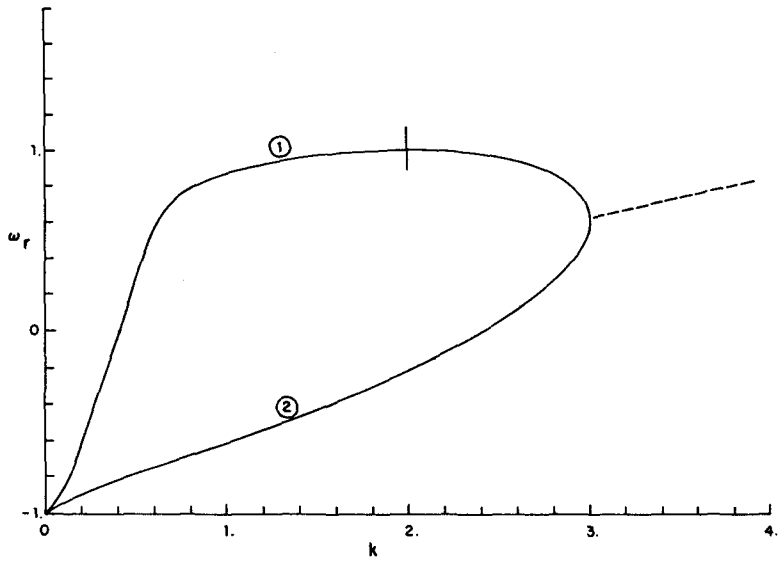

FIG. 3. Real frequency, ω_r, vs horizontal wavenumber, k, for $\Delta\bar{T} = 0$, $B_- = 2$, $R = 1$ and $\sigma = 0$. The solid curves are neutral and the dashed unstable.

comes unstable. Cairns states that a mode with negative energy calculated with respect to some frame of reference may be expected to become unstable by the extraction of energy by a dissipation process. Mode (1) is not negative with respect to the motionless interior, but is negative for $k > 2$ calculated with respect to the moving frame of the mean flow in the mixed layer. This is called a class A instability by Benjamin.

For our system this latter type is important since the magnitude of the instability is significant for small σ. The instability will not continue growing forever with increasing σ, but it will reach a maximum for given parameters and then decrease. Figure 4 for $\sigma = 0.1$ shows that these instability mechanisms merge together. Figure 5 shows the locus of the points of coalescence for the class C instability (dashed) for $\sigma = 0$ and the neutral curve ($k = 2f\bar{h}/k$) for $\sigma > 0$ and $\sigma \to 0$ of the class A instability (solid) in (R, k) space. It shows that the class A is more unstable than the class C in the sense that the critical value for R is less.

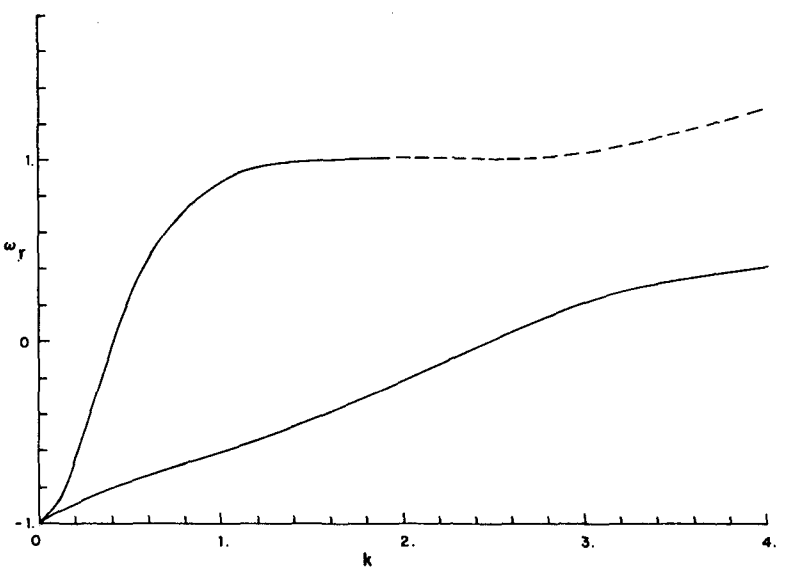

FIG. 4. As in Fig. 3, except $\sigma = 0.1$ and the solid curves are stable and the dashed unstable.

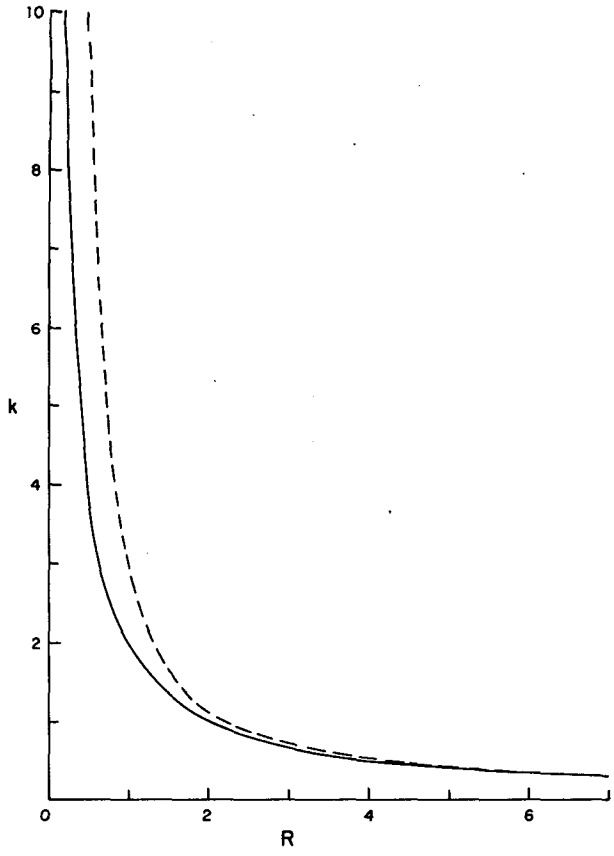

FIG. 5. Neutral stability curves with dashed for $\sigma = 0$ and solid for $\sigma > 0$ but approaching 0.

In summary, the short-wave instability is similar to the viscous parallel flow instability described by Lilly for the laminar problem. It behaves like a merger of class A and C instabilities as defined by Benjamin and it is similar to the instability described by Ostrovskiy and Tsimring.

The long-wave instability appears to be analogous to the inflection point instability described by Lilly (1966) for the laminar Ekman layer and by Stern (1977) Kamachi and Grimshaw (1984) for an inviscid rotating vertical shear model. But the mechanism is not the same. The important $w\bar{u}_z$ term in the vertical shear model is suppressed in our viscous two layer model, but the term $(-h/\bar{h}^2\tau^0)$ in (9a), produced by the perturbation of the mixed layer depth in the stress term, seems to play a similar role. We can show that there is a relationship between these terms.

Consider the case where the surface stress is in the negative x-direction ($\theta = 180°$) and $(\bar{u}, \bar{v}) = [0, (\tau_0/\bar{h}\rho_0 f_0)]U(z+\bar{h})$ in dimensional terms where $U(z+\bar{h})$ is the unit step function. If we were considering an inviscid shear model, we would have from (1a), eliminating v, the perturbation equation

$$u_{tt} + f_0^2 u = -\frac{1}{\rho_0} p_{xt} - f_0 w \bar{v}_z. \tag{17}$$

On the other hand, for our viscous system, we have from (9a), eliminating v, and neglecting irrelevant terms,

$$u_{tt} + f_0^2 u = -\frac{1}{\rho_0} p_{xt} + \frac{h_t}{\rho_0 \bar{h}^2} \tau_0. \tag{18}$$

So it is the comparison of the last terms of each of these equations which is of interest. If we average the last term of (17) over the mixed layer (integrating from just beneath the mixed layer), we obtain

$$\frac{1}{\bar{h}} \int_{-\bar{h}}^{0} -f_0 w(z) \bar{v}_z dz = \frac{-1}{\bar{h}} \int_{-\bar{h}}^{0} f_0 \frac{\tau_0}{\bar{h}\rho_0 f_0} \times \delta(z+\bar{h}) w(z) dz = \frac{-w(-\bar{h})\tau_0}{\rho_0 \bar{h}^2}, \tag{19}$$

where $\delta(z+\bar{h})$ is the Dirac-delta function. Since $w(-\bar{h}) = -h_t$, equation (19) becomes $h_t\tau_0/(\rho_0\bar{h}^2)$ which is the same as the term in (18). Thus the effect of the $w\bar{u}_z$ term in the inviscid model, which would be nonzero only in the transition layer, is distributed throughout the mixed layer in our formulation of the viscous problem in the form of a perturbation of the vertical gradient of stress. Our long-wave instability is then related to that of the inviscid shear model, but results will not be exactly the same because of the differing assumptions in handling the limiting process in the transition layer. Let us compare the results.

If we assume $\theta = 180°$, $\Delta\bar{T} = \sigma = 0$ in (16b), we obtain

$$\sqrt{\omega^2 - f^2} = \frac{1}{2}\left\{-i\bar{h}kB_- \pm \left[-\bar{h}^2k^2B_-^2 + 4\left(\frac{ikR\tau_0}{\bar{h}} + \bar{h}k^2B_-^2\Delta\bar{T}\right)\right]^{1/2}\right\}. \tag{20}$$

Furthermore, choosing the + sign in (20) which will give an unstable solution, we can show

$$\mathrm{Im}(\omega^2 - f^2) = \frac{\tau_0^2 R^2}{\bar{h}^4 B_-^2} s\left\langle 1 - \frac{1}{\sqrt{2}}\left\{\left[s^2 + \left(\frac{s^2}{4} - s^2 \times \frac{\Delta\bar{T}}{\bar{h}}\right)^2\right]^{1/2} - \left(\frac{s^2}{4} - s^2\frac{\Delta\bar{T}}{\bar{h}}\right)\right\}^{1/2}\right\rangle \tag{21}$$

where $s = kB_-^2\bar{h}^3/R\tau_0$. In dimensional terms this becomes

$$s = kN_-^2h^3(\tau^0/\rho_0) = kh^2N_-^2/f_0U^0$$

where $U^0 = \tau^0/\rho_0 f_0 h$ is the Ekman flow. If $\mathrm{Im}(\omega^2 - f^2) > 0$, the solution is unstable which implies instability for $s < (\bar{h}/\Delta\bar{T})^{1/2}$. For $\Delta\bar{T} \to 0$ it is unstable for all k. From (18) we can show that for $\Delta\bar{T} = 0$, ω_i is a maximum of $\approx 0.22/\bar{h}^4$ at $s \approx 1.95$ implying $k \approx 1.95/R\bar{h}^3$ (setting $B_- = R$). For the conditions of Fig. 2, $R = \bar{h} = 2$, the above would give a maximum of ω_i of about 0.013 at $k \approx 0.12$. This compares with Fig. 2, where we have friction, which shows a maximum around 0.0095 for $k \approx 0.22$.

For a slab profile in the inviscid shear model, Stern (1977) obtains, in dimensional terms, $k = (2/\pi)U^0 f_0/h^2 N_-^2$ for neutral stability, and it can be shown to be unstable for decreasing k. The balance here is the same as above for our long-wave instability except $s = 2/\pi$ rather than 1.95. The forces involved are mean shear, buoyancy and Coriolis where s can be written as a product of hN_-/U^0, the ratio of buoyancy to mean shear (the square root of a Richardson number), and khN_-/f_0, the ratio of buoyancy to Coriolis (the square root of a Burger number). For the Stern model ω_i is a maximum when $s = 1/\pi$, so for $R = \bar{h} = 2$, it gives a maximum $\omega_i = 0.001$ for $k = 1/\pi\bar{h}^3 R \approx 0.018$ in dimensionless terms.

In summary, our long-wave instability depends on a perturbation of the bulk stress, but it is related to and behaves like the inviscid inflection point instability with the same balance of forces. However, for comparable parameters our model predicts a stronger instability at a smaller wavelength than the other. Figure 6 shows how the wavelength, λ, and ω_i vary with N_-/f_0 for realistic parameters. Most realistically N_-/f_0 is between 100 and 200, so λ between 25 and 30 km would be expected.

Our two instabilities behave strikingly different as $\Delta\bar{T}$ is increased from zero. From results from (I) we can show that for no friction we must have $\Delta\bar{T} < 1/\bar{h}^3$ for the existence of the short-wave instability. For the conditions of Fig. 2, which includes friction, we must have $\Delta\bar{T} \leqslant 0.032$. On the other hand, for the long-wave instability, we can show that we must have $k < 1/\bar{h}^{5/2} R\sqrt{\Delta\bar{T}}$ for instability with no friction implying instability always exists for finite $\Delta\bar{T}$. For the conditions of Fig. 2, the long-wave instability eventually does disappear but not until $\Delta\bar{T} \gtrsim 1.5$. Thus the contrast is that, though the short-wave instability is much the stronger of the two for $\Delta\bar{T} = 0$, it is also much more sensitive to the stabilizing effect of increasing $\Delta\bar{T}$, disappearing quite quickly. For realistic deepening, where $\Delta\bar{T} \approx 0.5\bar{h}$, only the long-wave instability would exist after the mixed layer reached its equilibrium of $\bar{h} \approx 2$. This contrast is illustrated on Fig. 7, starting at the relative maximums of each instability at $\Delta\bar{T} = 0$ on Fig. 2 and increasing $\Delta\bar{T}$. (The results are for a relative maximum for only $\Delta\bar{T} = 0$.)

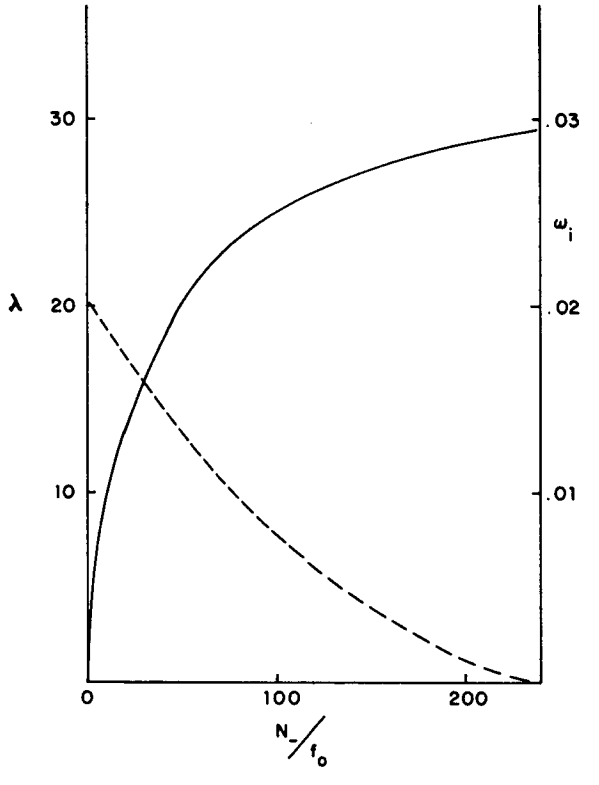

FIG. 6. The wavelength, λ, (solid) and ω_i (dashed) vs N_-/f_0 for the long wave instability with $\bar{h} = 2.0$, $\Delta\bar{T} = 2.0$, $\sigma = 0.0$, $C_D = 10^{-3}$, $\tau^0/\rho_0 = 2\,(\text{cm s}^{-1})^2$, $\theta = 221°$, $a = 0$, and ω_r very close to 1, throughout.

b. *Inclusion of steady-state oscillations*

Let us now include inertial oscillations in the mean flow by letting $a \neq 0$ in (13). We especially desire to know how the instabilities on Fig. 2 behave for increasing a and whether a parametric instability exists. In the previous work of (II) essentially only the $\theta = 90°$ case was considered, conditions for the short wave.

As in (II), we use Floquet theory for the solution. We assume the solution is a sum of inertial frequency harmonics having the form

$$( ) = \sum_{n=-\infty}^{\infty} (\hat{})_n e^{i(nf-\omega)t+ikx} \tag{22a}$$

in the mixed layer, and

$$( ) = \sum_{-\infty}^{\infty} (\hat{})_n e^{i\mu_n z} e^{i(nf-\omega)t+ikx} \tag{22b}$$

in the interior where $\mu_n^2 = B_-^2 k^2/[(\omega - nf)^2 - f^2]$. Since $\bar{h}_t = Q_0 = 0$, we again have $T = H = 0$ from (9c) and (9d). The solution follows similarly to our previous work where we generate an infinite determinant which must be suitably truncated to find numerical values for $\omega = \omega_r + i\omega_i$ in terms of the parameters. See (II) for the details.

Since we have a linear system with sinusoidally oscillating coefficients, we might expect the possibility of the existence of parametric instabilities. Our system is complicated and does not reduce to Mathieu's equation. In (II) it was thought a parametric instability existed because an instability was found to exist which became more unstable when the parameter equivalent to a was increased and which was not continuous with the instability for $a = 0$. However, θ was kept constant at 90° in (II). In calculations made with varying θ, we found that in every case examined the instability was continuous in some connected region in (θ, k) space

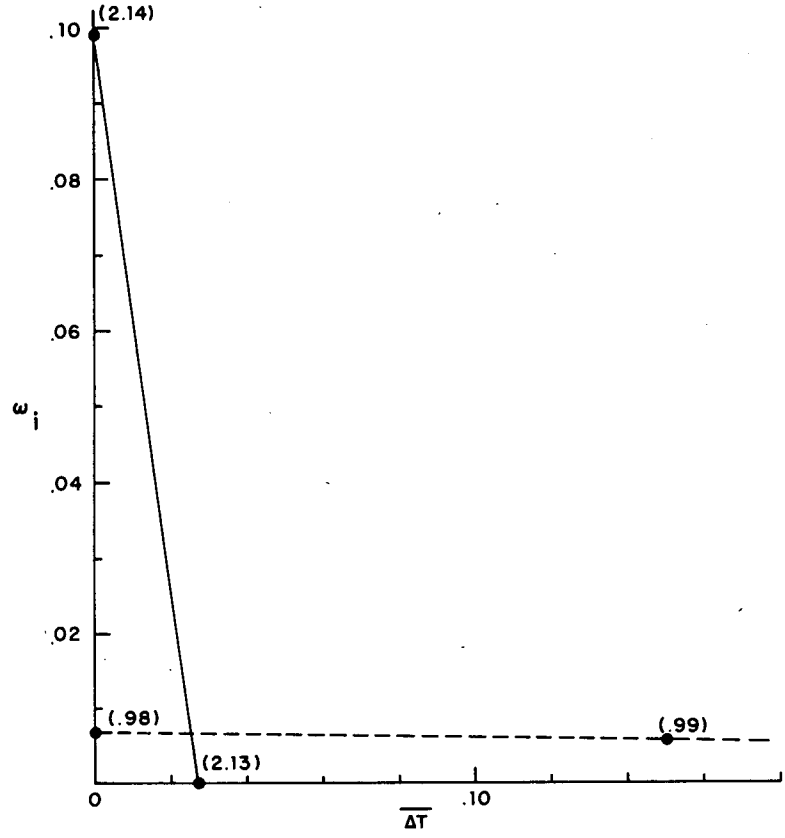

FIG. 7. ω_i vs $\Delta\bar{T}$ for the short-wave instability (solid) with $k = 4.0$ and $\theta = 92°$ and the long-wave instability (dashed) with $k = 0.22$ and $\theta = 198°$. In each case $\bar{h} = R = 2.0$, $a = 0$, $\sigma = 1$ and $\bar{\sigma} = 0.1$. The numbers in parentheses are values of ω_r.

for a increasing from 0 and became more stable for increasing a if we assume $\tau_0 = \sqrt{1 - a^2}$. This assumption for τ_0 implies that the kinetic energy in the mean flow remains constant and a change in a changes the partition of kinetic energy between the steady and oscillating parts. So we conclude that energy in the steady mean is more effective in creating an instability, and a parametric instability was not found.

Figure 8 illustrates how our instabilities in Fig. 2 decrease with increasing a for $\tau_0 = \sqrt{1 - a^2}$. The maximum instabilities do not remain at the same point in (θ, k) space as a increases. For example at $a = 0.6$, ω_i for the short-wave instability is a maximum at $\theta = 90°$, $k = 4.6$ where $\omega = 1.14 + 0.054i$ and ω_i for the long-wave instability is a maximum at $\theta = 192°$, $k = 0.18$ where $\omega = 0.993 + 0.0012i$. However, the maximums definitely decrease with increasing a. (That ω_i vanishes at about the same a in Fig. 8 for each is coincidental.)

On Fig. 8 we see that the frequency (ω_r) is not very near-inertial for the short wave instability. However, as a increases, the coefficient of the sum in (22) associated with $\omega_r - f$ becomes dominant for the kinetic energy density. For example, at $a = 0.5$ the dominant term has a frequency of 0.93. In general, as a increases, the dominant frequency of the energy density tends toward near-inertial. The dominant frequency of the energy flux does not, as explained in (II), since the vertical group speed decreases as $\omega_r \to f$. This is illustrated on Fig. 9 where we see that near-inertial frequency of 1.14 dominates the energy density but a frequency of 3.14 dominates the flux.

The conditions for Fig. 9 are those of the maximum of the short-wave instability at $a = 0.6$. The figure is similar to figures in (II). Frequencies for $n \leqslant 0$ predominate because the preferred direction of the most unstable wave is that of the steady mean flow. When there is no steady mean ($a = 1$) the figure becomes symmetric in n similar to Fig. 5 of (II). The long-wave instability at $a = 0.6$ for the same parameters of Fig. 9 at conditions of maximum instability ($\omega = 0.993 + i0.0012$ at $\theta = 192°$, $k = 0.18$) contrasts sharply with the short wave. Only the near-inertial term ($n = 0$) is significant for the energy density and only the near-inertial and the first overtone ($\omega = 1.993$) are significant for the flux.

This contrast seems to be general, based on other calculations. The reason is that the long wave instability is so weak. The implication of this is that the kind of

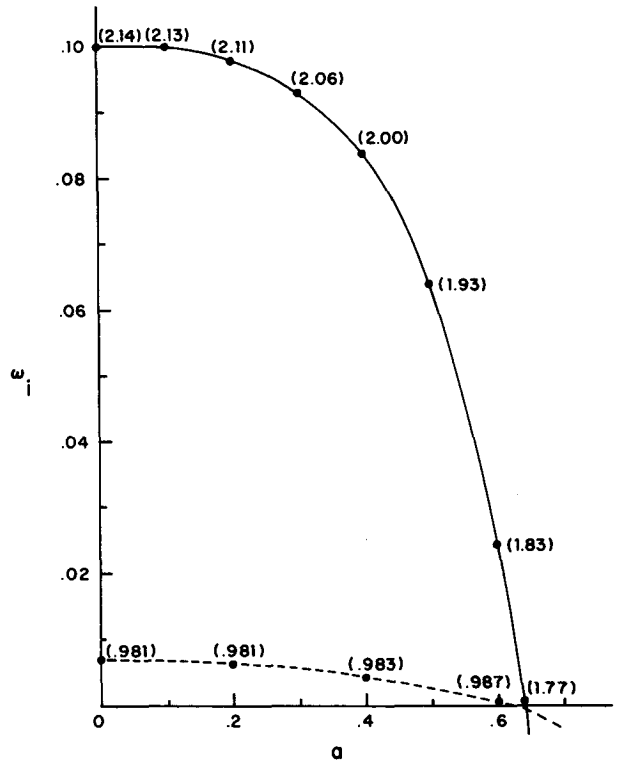

FIG. 8. ω_i vs a for the short-wave instability (solid) with $k = 4.0$ and $\theta = 92°$ and the long-wave instability (dashed) with $k = 0.22$ and $\theta = 198°$. In each case $\bar{h} = R = 2.0$, $\Delta\bar{T} = 0$, $\sigma = 1.0$, $\bar{\sigma} = 0.1$, and for this case $\tau_0 = \sqrt{1 - a^2}$. The numbers in parentheses are values of ω_r.

near-inertial overtone phenomenon observed by Pinkel and Titov (1973) could be caused by the short-wave instability but not the long-wave instability.

We found that shifting the partition of energy in the mixed layer into the oscillations stabilized both the long and short wavelength instabilities. If instead we add oscillations to a given steady mean flow, the long-wave instability will still stabilize while the short one will become more unstable. This is illustrated in Fig. 10. The instability for the short wave instability increases almost explosively. However, if the energy were added to the steady mean rather than as oscillations, it would be even greater. So it still holds that energy in the mean part is more destabilizing than energy in the oscillating part.

Figure 7 shows how quickly the short-wave instability disappeared as $\Delta\bar{T}$ increased. Since nominally we have $\Delta\bar{T} \approx 0.5\bar{h}$ and the steady state system does not approach equilibrium until $\bar{h}$ approaches 2, there is a question whether the short-wave instability will actually appear in nature. Figure 11 shows the variation of ω_i with $\bar{h}$ for the relative maximum for each instability for realistic parameters. It clearly shows that the short-wave instability disappears when $\bar{h}$ approaches 2. The long-wave instability is realistic in wavelength ($\sim$20 km) and is inertial, but is quite weak for $\bar{h} \approx 2$. For $\omega_i \sim 0.005$ we would have an increase in the amplitude by a factor of e in about 32 inertial periods. As $\bar{h}$ decreases from 1.0, the relative maximum which is the long-wave instability ceases to exist and the very strong short-wave instability dominates.

The conditions for Fig. 11 would be called usual. Hence it appears that under usual conditions the short wave instability will not occur. How extreme must they be for its occurrence? The most critical parameter is $\Delta\bar{T}$. In Fig. 12 we let $\Delta\bar{T} = 0.1\bar{h}$, and decrease friction, increase the wind, stratification and oscillations. The short wave instability does exist here for $\bar{h} = 2$, and it disappears quickly as $\bar{h}$ increases past 2.1. Here $\Delta\bar{T}$ is a fifth of that used for Fig. 11. This may be possible if there is significant surface cooling.

Pinkel (1983) has observed two groups of near-inertial waves at the same time and place with a longer (25 km) and shorter (8 km) wavelength. It is tempting to believe that these are our two instabilities. However, Weller (1985) believes that the scale and intensity of the observations are due to interaction with a significant

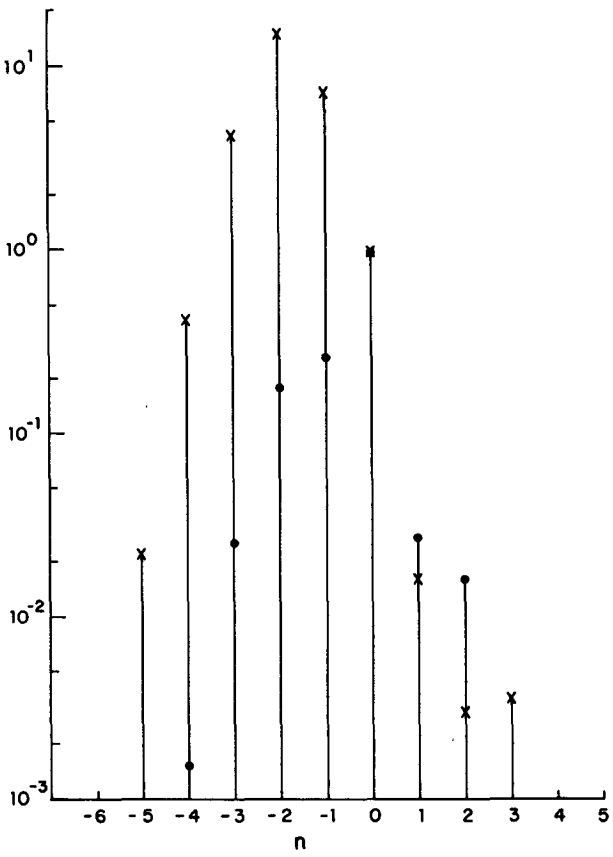

FIG. 9. The kinetic energy density, ($\cdot$) and the energy flux (x) for inertial harmonics (n) for $\omega = 1.137 + 0.054i$, $\tau_0 = \sqrt{1 - a^2}$, $a = 0.6$, $R = \bar{h} = 2.0$, $\Delta\bar{T} = 0.0$, $k = 4.6$, $\theta = 92°$, $\sigma = 1.0$ and $\bar{\sigma} = 0.1$. The values have been normalized by the value for $n = 0$. The frequency corresponding to each n is $\omega_r - nf$.

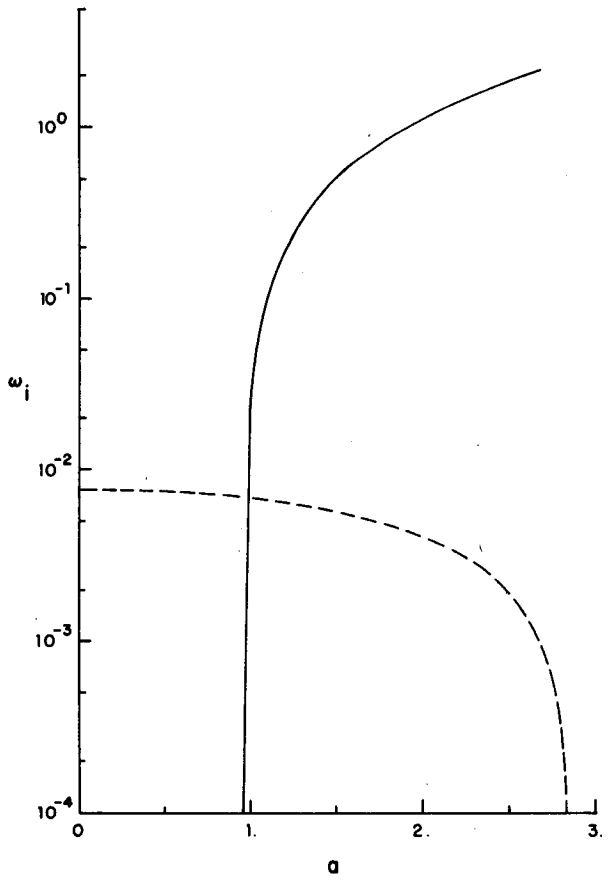

FIG. 10. ω_i vs a for the short-wave instability (solid) with $k = 7.3$, $\theta = 88°$, $R = 3$ and $\Delta\bar{T} = 0.2$, and for the long instability (dashed) with $k = 0.26$, $\theta = 221°$, $R = 1.4$ and $\Delta\bar{T} = 1.0$. In each case $\bar{h} = 2.0$, $\sigma = \bar{\sigma} = 0.1$ and $\tau_0 = 1.0$.

geostrophic shear current at the surface. Moreover, our short wave instability seems too short, being closer to 1 km than 8 km.

The wavelength can be increased by increasing K_H and increasing the a. It is possible for the steady state oscillations to be significantly larger than the mean part. Data of Pollard (1980), for example, indicate that a could be as large as 3. On Fig. 13 we show the real and imaginary parts of ω at the point of maximum instability versus a for $K_H = 10^6$ cm^2 s^{-1}. Here the wavelength varies between 2 and 3 km and the angle between 83° and 89°. A jump in ω_r occurs on this figure when a different relative maximum becomes the absolute maximum.

7. Summary and conclusions

A stability analysis of the Niiler mixed layer model yields two basic instabilities. One is a mixture of a Kelvin–Helmholtz type and a parallel flow viscous type which has a relatively small horizontal wavelength, O(1 km), for realistic conditions and whose most unstable wave is directed approximately along the mean flow. The second depends on the perturbation of the stress but is shown to be related to the inflection point type of instability. It has a relatively long horizontal wavelength, O(10 km), for realistic conditions with its most unstable wave directed approximately against the wind, perpendicular to the mean flow. For each of the instabilities the most unstable waves usually have a near-inertial frequency for realistic conditions.

For realistic conditions, the long wavelength instability is much more likely to be present than the other as exemplified by Fig. 11. This is because the short wavelength instability is stabilized very quickly with increasing temperature difference across the interface, $\Delta\bar{T}$, which realistically increases for increasing mixed layer depth. In contrast the long-wave instability is stabilized to a much smaller degree, exemplified by Figs. 7 and 11. The wavelength for the long-wave instability is consistent with observations (Sanford, Pinkel) with magnitudes from 20 to 30 km for realistic conditions as exemplified by Fig. 6. The instability is weak, how-

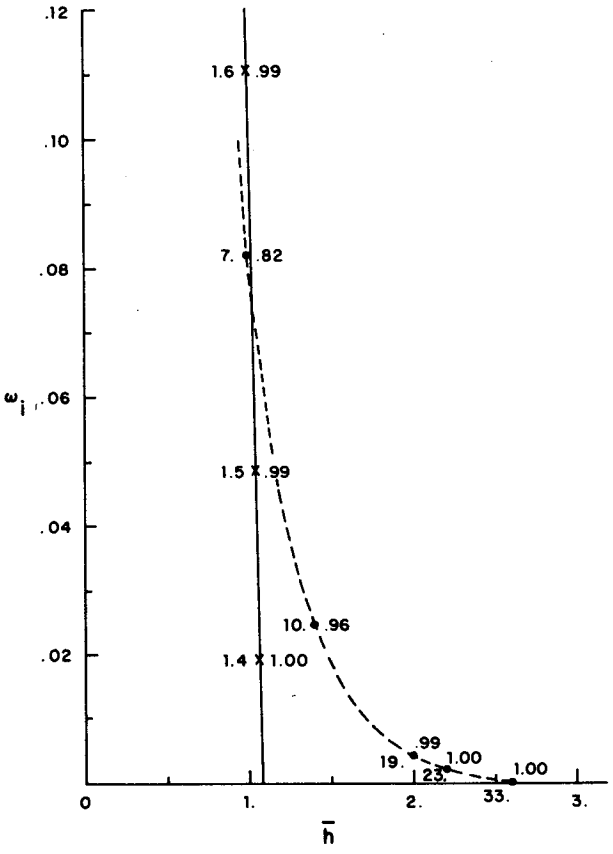

FIG. 11. The maximum value of ω_i vs $\bar{h}$ for the short wave instability (solid) with $\theta \approx 77°$ and the long wave instability (dashed) with $\theta \approx 215°$. For each case $\tau_0 = 1.0$, $\Delta\bar{T} = 0.5\bar{h}$, $a = 1.0$, $R = 1.0$, $\sigma = 1.0$ and $\bar{\sigma} = 0.1$. The numbers above or to the right of the curves are the values of ω_r; those below or to the left are the wavelength, λ in kilometers at the maximum.

ever, with an increase by a factor e taking O(20) inertial periods. In contrast, if the short-wave instability is present, it is much stronger as exemplified by Fig. 12. It seems possible that the short-wave instability can exist for unusual and extreme conditions such as an unusually strong steady-state flow or an unusually small temperature jump or a combination.

The two instabilities also contrast sharply in how they are affected by oscillations in the steady state. The long-wave instability is stabilized by an increase in oscillations while the short-wave instability becomes more unstable as exemplified by Fig. 10. However, there is no evidence of a parametric instability in the system. The short-wave instability produces strong near-inertial harmonics consistent with the observations of Titov and Pinkel while the long one does not. The basic conclusion of this analysis is that the characteristics of the models of Stern (1977) and the one of this author are both present in a more realistic model, with the former being the more likely to be observed. It is also noteworthy that this relatively simple model is still sufficiently robust to contain both types.

In this analysis we have examined solely the case for a fixed depth $\bar{h}$ with $\bar{h}_t = 0$. In a subsequent paper we will examine effects of deepening ($\bar{h}_t > 0$). We will see that the two instabilities discussed here are modified in important ways, and also that there are possibly important new instabilities generated.

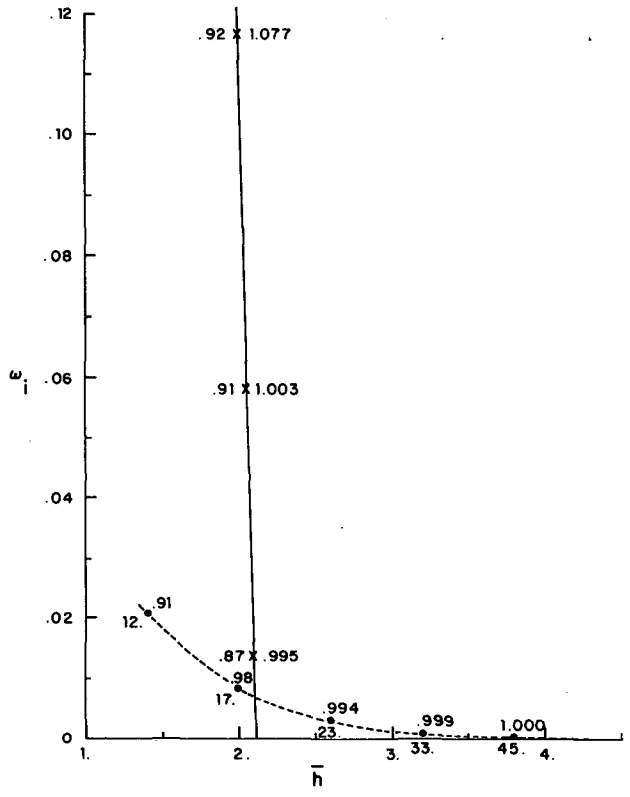

FIG. 12. As in Fig. 11 except $\Delta\bar{T} = 0.1\bar{h}$, $a = 1.5$, $R = 2.0$, $\sigma = 0.1$, $\bar{\sigma} = 0.2$.

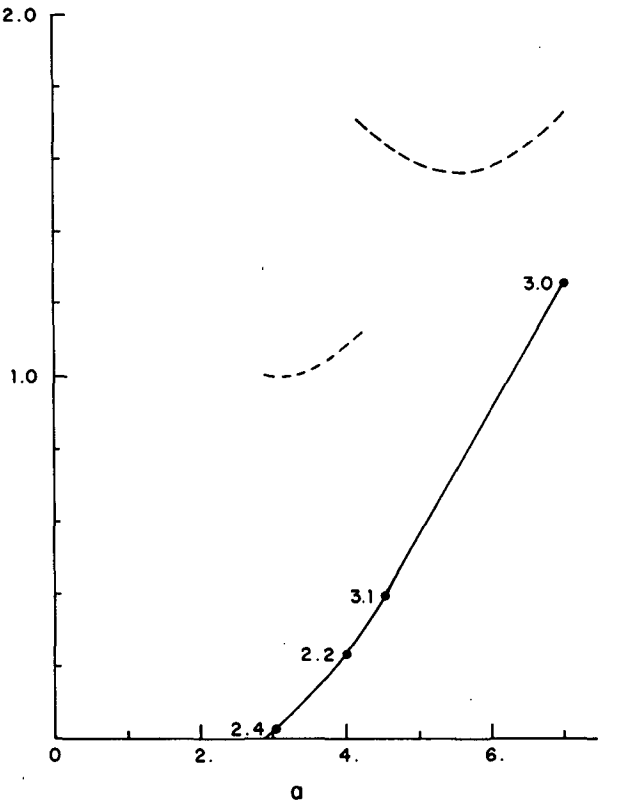

FIG. 13. The maximum value of ω_i (solid) and the value of ω_r (dashed) at the maximum vs a for $\Delta\bar{T} = 0.2$, $\bar{h} = 2.0$, $\tau_0 = 1.0$, $\sigma = 1.0$ and $\bar{\sigma} = 0$ for the short-wave instability. $83° < \theta < 89°$ throughout. The numbers above the ω_i curve are wavelengths (kilometers) at the maximum.

Acknowledgments. This work was supported by a Senior Research Associateship administered by the National Research Council at the Naval Postgraduate School, Monterey, CA.

REFERENCES

Alexander, R. C., and J.-W. Kim, 1976: Diagnostic model study of mixed-layer depths in the summer North Pacific. *J. Phys. Oceanogr.*, **6**, 293–305.

Benjamin, T. B., 1963: The threefold classification of unstable disturbances. *J. Fluid Mech.*, **16**(3), 436–443.

Bell, T. H., 1978: Radiation damping of internal oscillations in the upper ocean. *J. Fluid Mech.*, **88**(2), 289–308.

Brown, E. D., and W. B. Owens, 1982: Observations of the horizontal interactions between the internal wave field and the mesoscale flow. *J. Phys. Oceanogr.*, **11**, 1474–1481.

Cairns, R. A., 1979: The role of negative energy waves in some instabilities of parallel flows. *J. Fluid Mech.*, **92**(1), 1–14.

D'Asaro, E. A. and Henry Perkins, 1984: A near-inertial wave spectrum for the Sargasso Sea in late summer. *J. Phys. Oceanogr.*, **14**, 489–505.

deSzoeke, R., 1980: On the effects of horizontal variability of wind stress on the dynamics of the ocean mixed layer. *J. Phys. Oceanogr.*, **10**, 1439–1454.

Kamachi, M., and R. Grimshaw, 1984: Over-reflection of internal-inertial waves from the mixed layer. *J. Fluid Mech.*, **141**, 179–196.

Kroll, John, 1975: The propagation of wind-generated inertial oscillations from the surface into the deep ocean. *J. Mar. Res.* **33**(1), 15–51.

——, 1982: An unstable uniform slab model of the mixed layer as a source of downward propagating near-inertial motion. Part 1: Steady mean flow. *J. Mar. Res.*, **40**(4), 1013–1033.

——, 1984: An unstable uniform slab model of the mixed layer as a source of downward propagating near-inertial motion. Part 2: Unsteady mean flow. *J. Mar. Res.*, **42**, 83–102.

Kunze, E., 1985: Near-inertial propagation in geostrophic shear. *J. Phys. Oceanogr.*, **15**(5), 544–565.

Lilly, D. K., 1966: On the instability of Ekman flow. *J. Atmos. Sci.*, **23**, 481–494.

Niiler, P. P., 1975: Deepening of the wind-mixed layer. *J. Mar. Res.*, **33**, 405–422.

Ostrovskiy, L. A., and L. Sh. Tsimring, 1981: Radiating instabilities of shear flows in a stratified fluid. *Izv. Atmos Oceanic Phys.*, **17**(7), 564–566.

Pinkel, R., 1983: Doppler sonar observations of inertial waves: Wavefield structure. *J. Phys. Oceanogr.*, **13**, 804–815.

Pollard, R. T., 1980: Properties of near-surface inertial oscillations. *J. Phys. Oceanogr.*, **10**, 385–398.

Sanford, T. B., 1975: Observations of the vertical structure of internal waves. *J. Geophys. Res.*, **80**(27), 3861–3871.

Stern, M. E., 1977: Interaction of inertia-gravity waves with the wind. *J. Mar. Res.*, **35**, 479–498.

Tai, C.-K., 1981: Wave over-reflection and small scale nongeostrophic instabilities. Reports in Meteorology and Oceanography, No. 14, Harvard University, 131 pp.

Titov, V. B., 1973: Some distinctive features of mesoscale motions in the sea. *Oceanology*, **13**, 794–789.

Weller, R. A., 1985: Near-surface velocity variability at inertial and subinertial frequencies in the vicinity of the California current. *J. Phys. Oceanogr.*, **15**, 372–385.